*Desalination and Water Treatment*
www.deswater.com

doi: 10.5004/dwt.2017.20164

63 (2017) 262–274
February

# Analysis of photocatalytic degradation of azo dyes under sunlight with response surface method

Zahra Minaii Zangi, Hossein Ganjidoust*, Bita Ayati

*Environmental Engineering Department, Faculty of Civil and Environmental Engineering, Tarbiat Modares University, Iran, emails: h-ganji@modares.ac.ir (H. Ganjidoust), z.minaii@modares.ac.ir (Z. Minaii Zangi), ayati_bi@modares.ac.ir (B. Ayati)*

Received 24 April 2016; Accepted 14 August 2016

**ABSTRACT**

After synthesizing evaporating induction by ammonia to build dopant, the response surface method and central composite design model were used to find the optimum conditions of Direct Blue 71 dye removal. This approach was also used to determine interaction design parameters (pH, dye concentration, Zn:Ti molar ratio, photocatalyst concentration and time). Results showed that $TiO_2$ doped activity was higher than that of $TiO_2$ under sunlight. Additionally, the obtained model shows a positive correlation between the experiment results and the predicted response surface method responses. The removal efficiency was found to be 87% at 6 h and 90% at 8 h in optimal dye removal conditions including a pH of 6.9, a photocatalyst concentration of 44.6 mg/m$^2$, a dye concentration of 53 mg/L, and a Zn:Ti of 0.53%.

*Keywords:* Central composite design; Zn-$TiO_2$; DB71; Optimization; photo-reactors

## 1. Introduction

Dyes play important roles in various parts of the textile industry. Dyes often are artificial and obtained from two sources of oil: intermediate level and coal tar [1]. Synthetic dyes have a high solubility in water. Approximately 15% of the world's dyes enter industrial wastewaters and the environment during the dying process. In addition to the textile industry, the leather, paper, food, and health industries, as well as light absorbing cells and electrochemical photovoltaic cells also have dye in their wastewaters [2].

Heterogeneous photocatalyst by semiconductors is a common treatment method derived from advanced oxidation types that shows great potential for monitoring organic contaminants in water [3]. In the past decade, numerous studies conducted by researchers around the world have examined the use of heterogeneous photocatalyst oxidation in the decomposition and mineralization process of particular pollutants [2]. Studies have also looked at light irradiation's effect on the photocatalyst activity of different forms of $TiO_2$ such as film [4], powder [5], nanotube [6], stabilized [7], and doped $TiO_2$ [8].

Stimulation of $TiO_2$ layers by UV light leads to excitement in the electron capacity layer by the absorption of the photon and its transport layer in the direction of stimulation. In this case, electron-hole pairs are generated at the nanoparticle level, and oxygen molecules hitting the surface capture these electrons. The material level is thus very active, so the water can be oxidized by it. Therefore, this way of dealing with organic carbon molecules could transform them into carbon dioxide, water, and other formats [9].

One of the main problems of using $TiO_2$ as catalyst is its low efficiency in the visible light spectrum, which is due to a quick remix of electrons and holes. $TiO_2$ is not active due to its large band gap in visible light, so it is not able to maximize its solar photocatalyst potential. Many methods have been applied to $TiO_2$ be help it attract visible low-energy photons; these methods include modifying the surface by organic materials, grafting with semi-conductors, and modifying the band gap. To modify the band gap and improve efficiency, and reduce electronic remix, transition metals can be added as a dopant to $TiO_2$ [10–12].

* Corresponding author.

Due to the overlap of the intermediate band (3d) titanium with an orbital of d level in the transition metals, using a suitable transition metal as a dopant improves $TiO_2$ performance [13]. In general, making dope with the $TiO_2$ and metal ion improves the potential in generated radicals and broadens the absorption spectrum, making it less likely that electrons will become inhibited by ions, other electrons, and the hole remix [2].

Many researchers have investigated the use of dopant for increasing the photocatalyst activity of $TiO_2$. For example, Narayana et al. [14] investigated the photocatalyst effect of Fe and Co doped with $TiO_2$ using dye removal at 100 mg/L green malachite with 0.1 g catalyst in pH 7.3 ~ 7.5 in the sun. The rate of dye removal with Fe-$TiO_2$ after 3 h was more than 98% and 86% with the Co-$TiO_2$. The kinetics of dye removal with the Langmuir–Hinshelwood model is justifiable based on study results. Reaction rates of dye removal remained constant with Fe-$TiO_2$ at 0.8 $h^{-1}$, using dopant Co-$TiO_2$ at 0.67 $h^{-1}$, and using pure $TiO_2$ at 0.31 $h^{-1}$. Therefore, the photocatalyst effect of Fe-$TiO_2$ is more than that of the other two catalysts.

Goswami and Ganguli [15] compared the effect of Fe-$TiO_2$ made with ferrous sulfate hepta hydrate and ferric nitrate nanohydrate. In their study, a 25-W mercury lamp served as a light source. The initial concentration of the dye solution 10–5 was considered; 2 g catalyst in 50 mL dye solution was mixed in; and aeration was conducted. The results show that dopant made with ferrous due to a further reduction of crystalline network $TiO_2$ has a better photocatalyst effect on the amount of dye removal within 80 min, while the amount of dye removal with the ferric dopant was 80%.

The amount of Congo red dye removal was also tested to examine the photocatalyst effect of titanium dioxide-sulfonic acid nanocomposite irradiated with visible sunlight. In this case, the amount of dye removed from the solution in a volume of 100 mL with a concentration of 40 mg/L, a catalyst of $TiO_2$/SA, 1.5 g/L, and neutral pH for 210 min was more than 90%. Furthermore, the $H_2O_2$ oxidizing effect on dye removal was studied using the previous terms but adding 20 mm hydrogen peroxide. The rate of dye removal in 100 min under the same conditions was also more than 90% [16].

Yousef et al. [17] revealed satisfactory photodegradation of azo dyes, reactive black5 (RB5), and methyl red (MR) after being subjected to photocatalytic degradation for 120 min when the temperature was between 24°C and 30°C. Twenty-five mg of nanocatalysts ($Cu_0$ NPs-decorated, carbon-doped $TiO_2$ nanofibers, and Cu-free carbon-doped $TiO_2$ nanofibers) were added to 50 ml (10 mg/l) of the prepared azo dyes. These aqueous solutions were magnetically stirred under sunlight radiation. The sample dye concentration was measured by an UV–vis spectrophotometer. The prepared nanofibers removed 83% from RB5 and 65% from MR after 2 h of reaction.

The photoactivity sensitivity of Cu-$TiO_2$/ZnO toward operating conditions in an advanced oxidation reaction for the photodegradation of two different dyes under visible light irradiation has been investigated. The Cu-$TiO_2$/ZnO photocatalyst presented a maximum removal efficiency of color (83.35%), chemical oxygen demand (COD) (73.54%), and total organic carbon (TOC) (54.46%) for methyl orange (MO) in degradation with a concentration of 20 mg/L, 0.7 mg catalyst, and pH 4 for 120 min. For methylene blue (MB) degradation, the maximum removal efficiency was color (75.50%), COD (68.00%), and TOC (46.41%) with a concentration of 20 mg/L, 0.7 mg catalyst, and pH 10 for 120 min [18].

There are many methods for making dopant including the sol-gel, ball milling, and flame methods. In this study, a dopant with different amounts of metal created by evaporation-induced synthesis was constructed. Concrete was chosen as a stabilizing platform because it is one of the most useful and important constitutive materials of treatment plants. It is also available, inexpensive, and it has a simple construction technology. The experimental design was performed by response surface method (RSM) in order to data analyze and optimize initial pH, photocatalyst concentration, pollutant concentration, time, and ratio of zinc to titanium in the dopant manufacturing stage in synthetic dye removal Direct Blue 71 (DB71) with eight aromatic rings and three benzene rings.

## 2. Materials and method

### 2.1. Materials

Materials used in this study include DB71 dye made from Alvan Sabet of Hamedan; titanium dioxide nanoparticles containing anatase to rutile with a ratio of 80 to 20 and a 21 nm diameter from US Research NANO Inc. of USA; ammonia from Merck Co. of Germany; Portland concrete and water to produce concrete; concrete epoxy super glue made from optimal concrete chemistry; mold oil; and distilled water.

Equipment used included a Cary 50 spectrophotometer Varian for measuring absorption; Fungilab UE-6SFD ultrasonic cleaners for dispersing nanoparticles of titanium dioxide; Metrohm 691 digital pH meter to determine the pH of samples; Kern PLS 360-3 digital scale; Technic AP 1400F aquarium water pump capable of transferring water to a height of 1.3 m and having a flow rate of 200 L/s; Atinan AP aeration pump to provide required oxygen for the photocatalyst process with a liter per minute aeration flow; TES 1333 solar meter to measure the intensity of solar radiation; and DEM-RED oven with heating capacity to 800°C with the ability to stabilize the nanoparticles.

### 2.2. Preparation of photocatalyst

In order to make nanocomposite by induction, the evaporating synthesis method with ammonia was used [19]. First, the ammonia was added to nano-$TiO_2$ to reach a pH of 10.5 and stirred, then the suspension was added to zinc solution to form a complex of zinc ammonium with two additional positive charge (white layer formation on nanocrystal of $TiO_2$ represents the desired complex formation). This solution was stirred for 24 h according to Eq. (1). In order to convert to hydroxide Zn (Eq. (2)), the solution was evaporated. Finally, to reach the thermal decomposition zinc hydroxide to zinc oxide (Eq. (3)), the nanocomposite was placed in the oven for 4 h at 450°C.

$$Zn^{2+} + NH_3 <--> Zn(NH_3)_4^{2+} \quad (1)$$

$$Zn(NH_3)_4^{2+} + 2HO^- \rightarrow Zn(OH)_2 + 4NH_3 \quad (2)$$

$$Zn(OH)_2 \rightarrow ZnO + H_2O \quad (3)$$

X-ray diffraction (XRD) analysis was used to determine the presence of crystalline phases of titanium dioxide in the dopant composite structure.

### 2.3. Photochemical reactor start-up

The photo reactor shown in Fig. 1 consists of several parts. The reactor core, in which the solar photocatalytic process was carried out, consists of a 40 cm base of stairs, 30 cm height, and 37° horizontal angles. It is made with metal cans and a corner stone grade 3 for the maintenance of five concrete stairs. The 24 × 12 × 4 concrete plates are made of cement, on which the stabilized nanoparticles were placed during photocatalyst. The plates are 2.5 cm apart, and the ends of each stair have a 4 cm overlap. The 5-L wastewater storage tank is made of galvanized reflected sunlight. To protect the reactor against wind, rain, and evaporation, ordinary 3 mm thick glass of 40 × 100 m and a 37° horizontal angle at the front of reactor is installed, along with two 40 × 80 cm plates at the sides and two 60 × 40 cm plates behind the reactor. The ordinary glass light transmission coefficient is for wavelengths longer than 350 nm, which is more than 90% or Pyrex. Pyrex was not used, however, due to inaccessibility of the required dimensions among domestic producers and high cost from foreign countries.

To achieve laminar flow, the maximum flow rate is 22.95 L/min. For this reason, a 13.5-W aquarium pump with a flow rate of 200 L/h and a pumping height of 1.3 m is installed. Air is blown through an aerator pump for the dissolved oxygen supply in water. All the mentioned parts are placed on the 40 × 80 × 120 cm chassis. Third grade canisters equipped with four wheels are installed for ease of movement. This study established the solar reactor at the geographical coordinates 510 22′ 95″ E and 350 43′ 12″ N and 1,776 m above sea level. The photo reactor under a 37° angle is oriented to the south and contains a solar meter to measure the intensity of solar radiation in the visible region. Among the methods of nanoparticle stabilization, including sol-gel, slurry, and mix, slurry was used due to improved efficiency and ease of implementation [13].

In supplying a sustainability photocatalyst on the concrete context, the durability of the consolidation method is important. In other words, the most important parameter in the coated photocatalytic reactor is the lack of decreasing efficiency of the system during continuous operation due to the separation of the particles from the substrate surface [20].

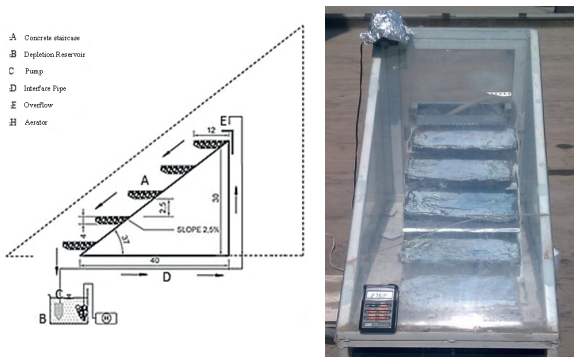


Fig. 1. Applied photo-reactor.

First, the glue was applied with a paint brush to a thickness of 5 mm on a concrete surface, and the $TiO_2$ suspension in a solution of distilled water-ethanol was produced. The solution was stirred for 10 min at 1,500 rpm and 200°C temperature. It remained in the ultrasonic cleaner for 20 min to separate aggregate nanoparticles and prepare a homogeneous suspension. After creating a homogeneous suspension, and 30 min after applying the glue, the concrete surface with suspension was submerged. It was dried for 72 h at room temperature in order to increase resistance against platform abrasion, and then heated in the oven at 1,500°C for 8 h.

### 2.4. The photocatalytic process

All tests were performed between 8 a.m. and 4 p.m. under sunlight, moderated at 1,004 W/m$^2$ and an average temperature of 35°C. Factors examined in this study included pH (6.9, [natural pH of dyes], 9, and 11), different molar ratios Zn:Ti (0.05%, 0.33%, 0.53%, 0.72%, and 1%), dye concentration (5, 20, 50, and 100 mg) and photocatalyst concentration (20, 50, and 80 g/m$^2$). To perform the tests, 3 L of synthetic wastewater (DB71 combination of dye and distilled water) was used. The percentage removal of dye at a rate of absorption at the wavelength of maximum absorbance (586 nm) using a spectrophotometer was determined.

## 3. Result

### 3.1. Characterization of Zn-$TiO_2$

Fig. 2 presents the XRD analysis of titanium dioxide nanoparticles. When comparing the samples' intensity of the characteristic peak of anatase (25.4, $I_A$) and rutile (27.4, $I_R$), the ratio of anatase to rutile phase ($I_R/I_A$) in doped samples appears to be fairly equal to the undoped sample, meaning the doping process inhibits anatase transmission to rutile [21]. It should be noted that the photocatalytic properties of anatase is superior to those of the rutile phase [22].

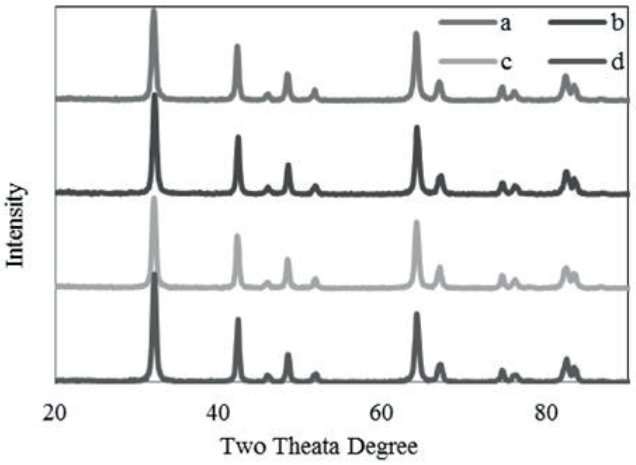


Fig. 2. XRD of: a – undoped $TiO_2$, b – 0.5% Zn-$TiO_2$, c – 0.6% Zn-$TiO_2$, and d – 0.72% Zn-$TiO_2$.

### 3.2. RSM model analysis

#### 3.2.1. Design

Table 1 presents the central composite design [23] table, along with the experimental and predicted responses. Point 38 in the model, removal of dye, and point 1, removal of organic load, were ignored. A quadratic equation was obtained for all three responses using the analysis of variance results with a 95% confidence level. Table 2 reports the standard errors, coefficients of reliability, sum of squares, and *F*-value. Eqs. (1)–(3), respectively, outline the proposed model for dye removal, removal of organic load, and the pH value of the output. The model related to the removal of organic load by removing two sentences $[Dye]^2$ and $[time]^2$ has been modified. Values of adjusted $R^2$ and $R^2$ are reported in Table 2.

$$\text{Dye removed \%} = -332.93216 - 0.74502 \times [\text{Dye}] + 1.86425 \times \text{pH} + 9.75641 \times [\text{ZnO-TiO}_2] + 37.74798 \times \text{Time} + 499.16242 \times [\text{Zn:Ti}] - 1.14883\text{E-}003 \times [\text{Dye}] \times \text{pH} + 0.010624 \times [\text{Dye}] \times [\text{ZnO-TiO}_2] + 0.022204 \times [\text{Dye}] \times \text{Time} - 0.40872 \times [\text{Dye}] \times [\text{Zn:Ti}] + 2.92746\text{E-}003 \times \text{pH} \times [\text{ZnO-TiO}_2] - 0.052473 \times \text{pH} \times \text{Time} - 1.27678 \times \text{pH} \times [\text{Zn:Ti}] - 0.065152 \times [\text{ZnO-TiO}_2] \times \text{Time} - 4.17371 \times [\text{ZnO-TiO}_2] \times [\text{Zn:Ti}] - 9.85275 \times \text{Time} \times [\text{Zn:Ti}] - 9.61007\text{E-}004 \times [\text{Dye}]^2 - 0.20428 \times \text{pH}^2 - 0.091253 \times [\text{ZnO-TiO}_2]^2 - 2.56921 \times \text{Time}^2 - 203.14123 \times [\text{Zn:Ti}]^2 \quad (4)$$

$$\text{COD removed \%} = -41.21921 + 0.38770\ [\text{Dye}] + 19.84771\ \text{pH} + 2.06753\ [\text{ZnO-TiO}_2] - 3.61193\ \text{Time} - 44.83242\ [\text{Zn:Ti}] - 0.069399 \times [\text{Dye}] \times \text{pH} - 1.35125\text{E-}003 \times [\text{Dye}] \times [\text{ZnO-TiO}_2] + 0.031382 \times \text{Dye} \times \text{Time} + 0.82185 \times [\text{Dye}] \times [\text{Zn:-Ti}] - 0.028452 \times \text{pH} \times [\text{ZnO-TiO}_2] - 0.63157 \times \text{pH} \times \text{Time} + 9.93383 \times \text{pH} \times [\text{Zn:Ti}] + 0.098725 \times [\text{ZnO-TiO}_2] \times \text{Time} - 0.43868 \times [\text{ZnO-TiO}_2] \times [\text{Zn:Ti}] + 1.21132 \times \text{Time} \times [\text{Zn:-Ti}] - 0.96218 \times \text{pH}^2 - 0.019572 \times [\text{ZnO-TiO}_2]^2 - 71.51145 \times [\text{Zn:Ti}]^2 \quad (5)$$

$$\text{pH-out} = +8.00944 + 0.016456 \times [\text{Dye}] - 0.26458 \times \text{pH} - 3.71064\text{E-}003 \times [\text{ZnO-TiO}_2] + 0.092280 \times \text{Time} + 1.52993 \times [\text{Zn:Ti}] - 5.95458\text{E-}004 \times [\text{Dye}] \times \text{pH} - 2.25778\text{E-}004 \times [\text{Dye}] \times [\text{ZnO-TiO}_2] + 1.91397\text{E-}004 \times [\text{Dye}] \times \text{Time} - 6.26798\text{E-}004 \times [\text{Dye}] \times [\text{Zn:Ti}] + 1.35529\text{E-}003 \times \text{pH} \times [\text{ZnO-TiO}_2] - 5.05076\text{E-}003 \times \text{pH} \times \text{Time} - 0.27726 \times \text{pH} \times [\text{Zn:Ti}] + 6.39763\text{E-}004 \times [\text{ZnO-TiO}_2] \times \text{Time} - 0.019849 \times [\text{ZnO-TiO}_2] \times [\text{Zn:Ti}] - 0.038279 \times \text{Time} \times [\text{Zn:Ti}] - 8.75158\text{E-}006 \times [\text{Dye}]^2 + 0.030953 \times \text{pH}^2 + 2.72505\text{E-}004 \times [\text{ZnO-TiO}_2]^2 - 6.10169\text{E-}003 \times \text{Time}^2 + 2.08423 \times [\text{Zn:Ti}]^2 \quad (6)$$

Fig. 3 presents the degree of dispersion of experimental data and predicted responses (indicating the $R^2$ coefficient). The dispersion of points around and below the 45° line indicates that the model predicted values are closer to reality and are more accommodating [24].

To use the model in the design space, the ratio of S:N (signal to noise) must be greater than 4 to achieve the model of dye removal of 15.83, the removal of organic load of 7.224, and the pH output of 6.661.

#### 3.2.2. Analysis of effective factors

After introducing the models and assessing their errors, the interaction of effective factors was investigated. Fig. 4 shows the effect of dye concentration and pH on the responses of dye removal, removal of organic load, and output pH in constant conditions of concentration: photocatalyst of 40 g/m$^2$, the Zn:Ti ratio equal to 0.5, pH 7, and duration of 5 h. Fig. 4(A) shows that, with increasing dye concentration and pH, the organic load removal efficiency of less than 36 increases to more than 90% because the complex building dye decreases. This results in an increased removal of organic load. Fig. 4(B) indicates that an increase in the acidic pH of the dye concentration increases output pH, and the alkaline pH leads to decreased output pH because the dye investigated has been anion and is buffered.

According to Fig. 4(C), as pH increases, dye removal decreases due to the decreasing complex building process. As dye is increased, efficiency decreases because there is insufficient reaction time to remove the dye [25,26].

Fig. 5 shows the effect of dye concentration and a photocatalyst on the responses' dye removal, and output pH during constant conditions (Zn:Ti ratio equal to 0.5, pH 7, and 5-h duration). Fig. 5(A) shows that the amount of photocatalyst in the dye removal reduces as dye concentration increases. This reduces the effect of the surface's number of active centers relative to the contaminant molecules. As Fig. 5(B) indicates, by increasing the amount of photocatalyst, output pH increases because the doped metal produces hydroxyl and oxygen radicals [27].

Fig. 6 shows the effect of dye concentration and the Zn:Ti molar ratio on dye removal responses and removal of organic load in constant conditions (photocatalyst concentration 40 g/m$^2$, pH 7, and 5-h duration). In Fig. 6(A), the increase in dye concentration decreases the effect of the Zn:Ti molar ratio in the removal efficiency because the number of hydroxyl radicals generated by doped metal rather than the pollutant molecules is decreased. In the composite $TiO_2$-ZnO, the electron transfers from the conduction band of excited ZnO to the conduction band of excited $TiO_2$ and vice versa; a cavity transfer can occur from the valence band ZnO to the valence band $TiO_2$; this effective separation increases the responsibility load of the composite photocatalytic. Therefore, the maximum photocatalytic activity was related to the amount of ZnO, which received electrons generated from the $TiO_2$ light excitation. Therefore, as Fig. 6(B) shows, when the optimum photocatalytic activity is approached, more electrons are generated, and the output pH decreases. Jiang et al. [28] reported similar results in their study.

Fig. 7 demonstrates the effect of the photocatalyst concentration and pH on dye removal responses and removal of organic load in constant conditions of dye concentration 40 mg/L, the Zn:Ti molar ratio equal to 0.5, and 5-h duration. Figs. 7(A) and (B) show that by increasing pH, dye removal efficiency decreases, and the organic load removal efficiency increases because the complex process decreases. The dye removal efficiency of the organic load increases with an increased concentration of photocatalyst, but after about 50 g/m$^2$, it is decreased since the increased photocatalyst leads to increased active surface sites, thereby increasing the

Table 1
CCD matrix

| Factor No. | Dye con. (mg/L) | pH | Photo catalysis ($g/m^2$) | Time (h) | Zn:Ti | Experimental | | | RSM | | |
|---|---|---|---|---|---|---|---|---|---|---|---|
| | | | | | | DR[a] % | CODR[b] % | pH-out | DR % | CODR % | pH-out |
| 1 | 33 | 5 | 37 | 3 | 0.33 | 54.6 | 59.2 | 8.3 | 55.1 | – | 8.3 |
| 2 | 72 | 5 | 37 | 3 | 0.33 | 29.1 | 88.4 | 8.6 | 34.3 | 86.3 | 8.5 |
| 3 | 33 | 9 | 37 | 3 | 0.33 | 42.5 | 92.4 | 8.6 | 50.0 | 87.8 | 8.6 |
| 4 | 72 | 9 | 37 | 3 | 0.33 | 27.0 | 91.1 | 8.8 | 29.1 | 91.7 | 8.7 |
| 5 | 33 | 5 | 63 | 3 | 0.33 | 39.1 | 85.3 | 9.1 | 40.9 | 74.9 | 8.8 |
| 6 | 72 | 5 | 63 | 3 | 0.33 | 31.7 | 86.7 | 8.8 | 30.8 | 86.8 | 8.7 |
| 7 | 33 | 9 | 63 | 3 | 0.33 | 44.2 | 72.2 | 9.4 | 36.1 | 87.2 | 9.2 |
| 8 | 72 | 9 | 63 | 3 | 0.33 | 19.5 | 96.5 | 9.1 | 25.8 | 89.7 | 9.1 |
| 9 | 33 | 5 | 37 | 6 | 0.33 | 77.6 | 42.5 | 8.4 | 82.8 | 67.6 | 8.4 |
| 10 | 72 | 5 | 37 | 6 | 0.33 | 61.8 | 93.3 | 8.5 | 64.6 | 84.5 | 8.6 |
| 11 | 33 | 9 | 37 | 6 | 0.33 | 73.4 | 88.9 | 8.8 | 77.3 | 76.1 | 8.7 |
| 12 | 72 | 9 | 37 | 6 | 0.33 | 52.0 | 6.1 | 9.2 | 58.9 | 83.7 | 8.8 |
| 13 | 33 | 5 | 63 | 6 | 0.33 | 57.8 | 96.0 | 9.2 | 63.8 | 76.8 | 8.9 |
| 14 | 72 | 5 | 63 | 6 | 0.33 | 52.6 | 75.3 | 8.9 | 56.3 | 92.3 | 8.9 |
| 15 | 33 | 9 | 63 | 6 | 0.33 | 63.6 | 65.1 | 9.3 | 58.5 | 82.8 | 9.3 |
| 16 | 72 | 9 | 63 | 6 | 0.33 | 42.6 | 98.2 | 9.0 | 50.8 | 89.0 | 9.2 |
| 17 | 33 | 5 | 37 | 3 | 0.72 | 87.3 | 56.8 | 9.2 | 87.0 | 51.9 | 8.9 |
| 18 | 72 | 5 | 37 | 3 | 0.72 | 48.5 | 69.3 | 9.2 | 59.7 | 78.2 | 9.0 |
| 19 | 33 | 9 | 37 | 3 | 0.72 | 80.7 | 78.2 | 9.1 | 80.2 | 80.0 | 8.8 |
| 20 | 72 | 9 | 37 | 3 | 0.72 | 49.6 | 90.5 | 8.8 | 52.8 | 97.0 | 8.9 |
| 21 | 33 | 5 | 63 | 3 | 0.72 | 33.0 | 23.5 | 9.0 | 30.7 | 49.3 | 9.1 |
| 22 | 72 | 5 | 63 | 3 | 0.72 | 10.2 | 81.3 | 9.1 | 14.1 | 74.2 | 9.1 |
| 23 | 33 | 9 | 63 | 3 | 0.72 | 16.5 | 78.2 | 9.4 | 24.2 | 74.9 | 9.2 |
| 24 | 72 | 9 | 63 | 3 | 0.72 | 9.2 | 91.1 | 9.4 | 7.5 | 90.6 | 9.1 |
| 25 | 33 | 5 | 37 | 6 | 0.72 | 95.1 | 46.1 | 9.1 | 103.1 | 47.8 | 8.9 |
| 26 | 72 | 5 | 37 | 6 | 0.72 | 72.3 | 81.8 | 9.1 | 78.4 | 77.8 | 9.1 |
| 27 | 33 | 9 | 37 | 6 | 0.72 | 94.2 | 50.8 | 8.8 | 95.9 | 69.7 | 8.8 |
| 28 | 72 | 9 | 37 | 6 | 0.72 | 59.5 | 86.2 | 8.9 | 71.0 | 90.3 | 8.9 |
| 29 | 33 | 5 | 63 | 6 | 0.72 | 44.8 | 41.3 | 9.3 | 42.1 | 52.6 | 9.2 |
| 30 | 72 | 5 | 63 | 6 | 0.72 | 20.9 | 75.8 | 9.4 | 28.1 | 81.2 | 9.2 |
| 31 | 33 | 9 | 63 | 6 | 0.72 | 28.3 | 77.0 | 9.4 | 35.0 | 72.0 | 9.2 |
| 32 | 72 | 9 | 63 | 6 | 0.72 | 20.9 | 92.2 | 9.3 | 20.9 | 91.3 | 9.1 |
| 33 | 5 | 7 | 50 | 5 | 0.53 | 98.9 | 81.4 | 8.3 | 99.2 | 67.8 | 8.7 |
| 34 | 100 | 7 | 50 | 5 | 0.53 | 76.6 | 91.6 | 8.6 | 57.6 | 106.4 | 8.7 |
| 35 | 53 | 3 | 50 | 5 | 0.53 | 95.0 | 70.1 | 8.8 | 84.6 | 57.0 | 9.1 |
| 36 | 53 | 11 | 50 | 5 | 0.53 | 78.3 | 86.4 | 9.1 | 70.0 | 86.4 | 9.4 |
| 37 | 53 | 7 | 20 | 5 | 0.53 | 55.4 | 77.5 | 8.3 | 36.7 | 67.9 | 8.6 |
| 38 | 53 | 7 | 80 | 5 | 0.53 | 47.2 | 74.6 | 9.1 | | 71.1 | 9.4 |
| 39 | 53 | 7 | 50 | 1 | 0.53 | 26.7 | 95.3 | 8.2 | 24.6 | 89.9 | 8.6 |
| 40 | 53 | 7 | 50 | 8 | 0.53 | 90.2 | 93.1 | 8.6 | 73.6 | 84.3 | 8.7 |

*(continued)*

Table 1 *(continued)*

| Factor No. | Dye con. (mg/L) | pH | Photo catalysis ($g/m^2$) | Time (h) | Zn:Ti | Experimental | | | RSM | | |
|---|---|---|---|---|---|---|---|---|---|---|---|
| | | | | | | DR[a] % | CODR[b] % | pH-out | DR % | CODR % | pH-out |
| 41 | 53 | 7 | 50 | 5 | 0.05 | 40.0 | 79.8 | 8.9 | 33.6 | 82.2 | 8.9 |
| 42 | 53 | 7 | 50 | 5 | 1.00 | 48.2 | 75.3 | 9.0 | 35.9 | 59.7 | 9.5 |
| 43 | 53 | 7 | 50 | 5 | 0.53 | 84.5 | 93.1 | 8.3 | 80.6 | 87.1 | 8.7 |
| 44 | 53 | 7 | 50 | 5 | 0.53 | 81.5 | 88.6 | 8.7 | 80.6 | 87.1 | 8.7 |
| 45 | 53 | 7 | 50 | 5 | 0.53 | 81.3 | 88.6 | 8.8 | 80.6 | 87.1 | 8.7 |
| 46 | 53 | 7 | 50 | 5 | 0.53 | 82.2 | 89.4 | 8.7 | 80.6 | 87.1 | 8.7 |
| 47 | 53 | 7 | 50 | 5 | 0.53 | 82.0 | 89.4 | 8.7 | 80.6 | 87.1 | 8.7 |
| 48 | 53 | 7 | 50 | 5 | 0.53 | 82.3 | 90.1 | 8.7 | 80.6 | 87.1 | 8.7 |
| 49 | 53 | 7 | 50 | 5 | 0.53 | 81.4 | 88.6 | 8.8 | 80.6 | 87.1 | 8.7 |
| 50 | 53 | 7 | 50 | 5 | 0.53 | 81.6 | 90.9 | 8.8 | 80.6 | 87.1 | 8.7 |

[a]DR: Dye removal.
[b]CODR: The expression of the removal of the organic matter.

Table 2
Analysis of variance

| Response | Source | Squares | *df* | Square | *F*-value | Prob > *F* | |
|---|---|---|---|---|---|---|---|
| DR | Model | 29,475.11 | 20 | 1,473.756 | 17.28648 | <0.0001 | Significant |
| | Residual | 2,387.136 | 28 | 85.25484 | | | |
| | Lack of fit | 2,379.479 | 21 | 113.3085 | 103.5942 | <0.0001 | Significant |
| | Pure error | 7.656409 | 7 | 1.093773 | | $R^2$ value = 0.9251 | |
| | Cor. total | 31,862.25 | 48 | | | $R^2$adj = 0.8716 | |
| CODR | Model | 7,906.20 | 18 | 439.23 | 2.59 | 0.0103 | Significant |
| | Residual | 5,088.25 | 30 | 169.61 | | | |
| | Lack of fit | 5,071.9 | 23 | 220.52 | 94.37 | <0.0001 | Significant |
| | Pure error | 16.36 | 7 | 2.34 | | $R^2$ value = 0.6084 | |
| | Cor. total | 12,994.45 | 48 | | | $R^2$adj = 0.37735 | |
| pH-out | Model | 3.454548 | 20 | 0.172727 | 2.451472 | 0.0136 | Significant |
| | Residual | 2.0433 | 29 | 0.070459 | | | |
| | Lack of fit | 1.8833 | 22 | 0.085605 | 3.7452 | 0.0396 | Significant |
| | Pure error | 0.16 | 7 | 0.022857 | | $R^2$ value = 0.683 | |
| | Cor. total | 5.497848 | 49 | | | $R^2$adj = 0.3720 | |

removal of dyes and organic load. However, if the amount of photocatalyst is much more efficient, photocatalyst particles agglomerate, and the number of active points decreases because light does not reach the compacted particles. This results in decreases in dye removal efficiency and organic load; Sajjad et al. [29] and Sun et al. [30] report similar results.

The interaction of two factors, pH and Zn:Ti, during a 5-h duration, photocatalyst concentration of 40 $g/m^2$, and dye concentration of 40 mg/L, is shown in Fig. 8, as well as its impact on dye removal, organic load removal, and output pH. Zinc ion as a dopant produces oxygen and hydroxyl radicals, which effectively reduces the dye amount [13]. Thus, when increasing the amount of zinc ion on dye removal, removal of organic load increases because the concentration of the doped $TiO_2$ is higher than optimal, the oxygen surface forms cavities, and $Ti^{3+}$ acts as a recombination center to decrease the doped samples' activity in visible light [11] (Figs. 8(A) and (B)). In Part C, the increase of Zn:Ti due to additional hydroxyl radical production causes pH output to increase.

In Fig. 9, the effect of the interaction between the dye concentration and duration on dye removal and removal of organic dyes has been shown, with a photocatalyst concentration of 40 $g/m^2$, pH 7, and Zn:Ti ratio equal to 0.5. The effect of the photocatalyst concentration on dye removal increases over time (Fig. 9(A)) and decreases the organic load degradation (Fig. 9(B)). The increase of time enables sufficient time for a reaction, but the production power of the radicals in a

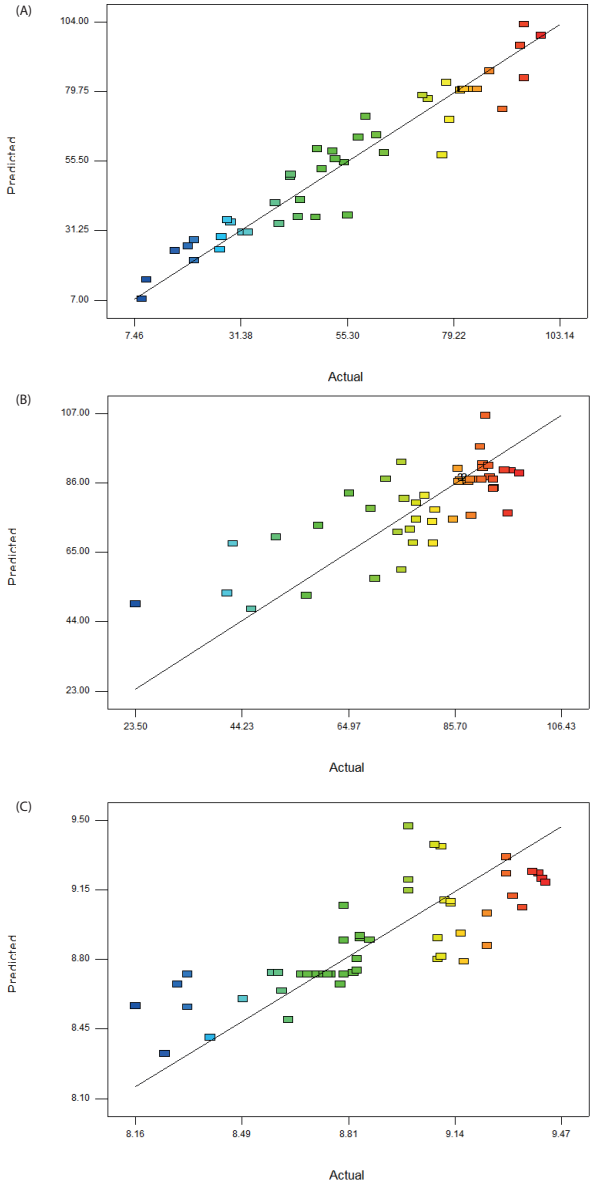


Fig. 3. The experimental response against the predicted values: (A) DR, (B) CODR, and (C) pH-out.

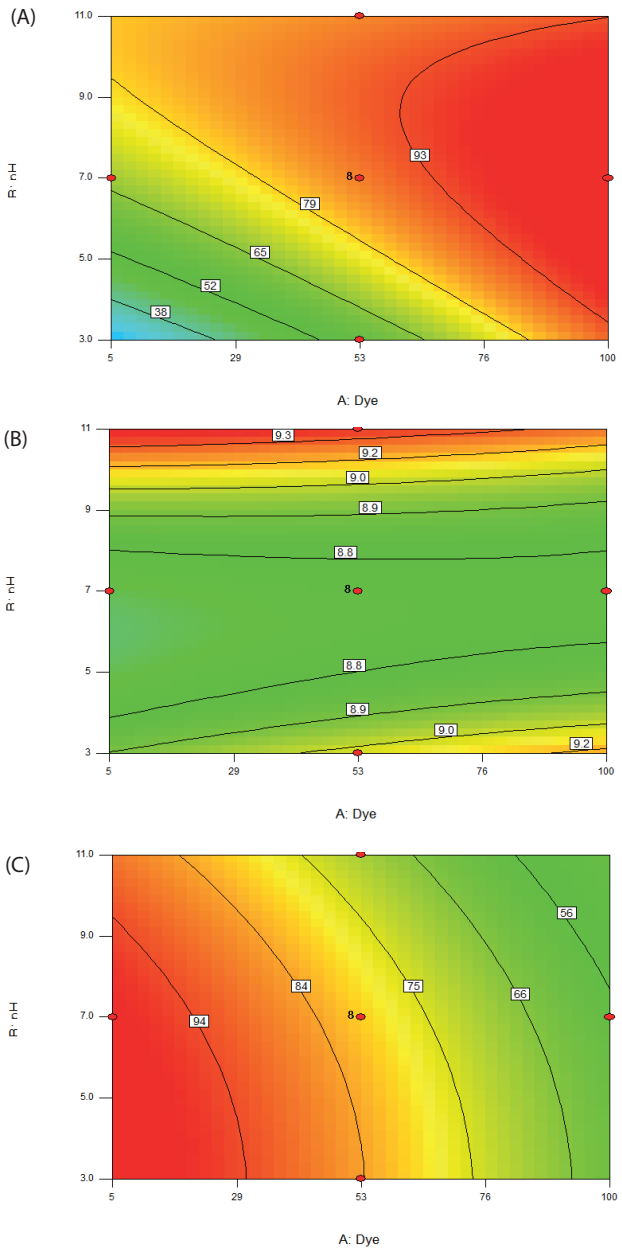


Fig. 4. Effect of initial dye concentration and pH: (A) CODR, (B) pH-out, and (C) DR ($t$ = 5 h, Zn:Ti = 0.5%, [Zn-$TiO_2$] = 40 g/$m^2$).

certain amount of metal (Zn:Ti fixed) does not increase with time; therefore, organic load removal will reduce [31].

Fig. 10 shows the interaction between the photocatalyst concentration and the Zn:Ti ratio on dye removal in constant conditions (5 h, 40 mg/L dye concentration, and neutral pH), indicating the reduction of the optimum photocatalyst amount with increasing Zn:Ti, because the metal doped photocatalytic activity exacerbates $TiO_2$ due to increased hydroxyl radical production [32].

Fig. 11 provides two-dimensional diagrams representing the effect of time and Zn:Ti on dye removal responses and output pH in constant conditions (photocatalyst concentration of 40 g/$m^2$ and dye concentration of 40 mg/L at neutral pH). By increasing time, the effect of the Zn:Ti ratio on dye removal increases because there is ample opportunity for response and increased radical production. In this case, output pH increases, similar to the results found by Nguyen et al. [32] and Rehman et al. [11].

### 3.3. The photocatalytic degradation of dye

#### 3.3.1. Effect of pH

Changes in pH solution changes $TiO_2$ particle surface charge and, consequently, catalytic reaction [33]. Fig. 12 outlines the results of pH changes at constant conditions. According to the results, the system's efficiency at pH 3 to 11 ranges from 90% to 40%, so a complete model is needed in all these areas. The $TiO_2$ surface below the ISO-electric point (6.8) is positive but negative above the ISO-electric point.

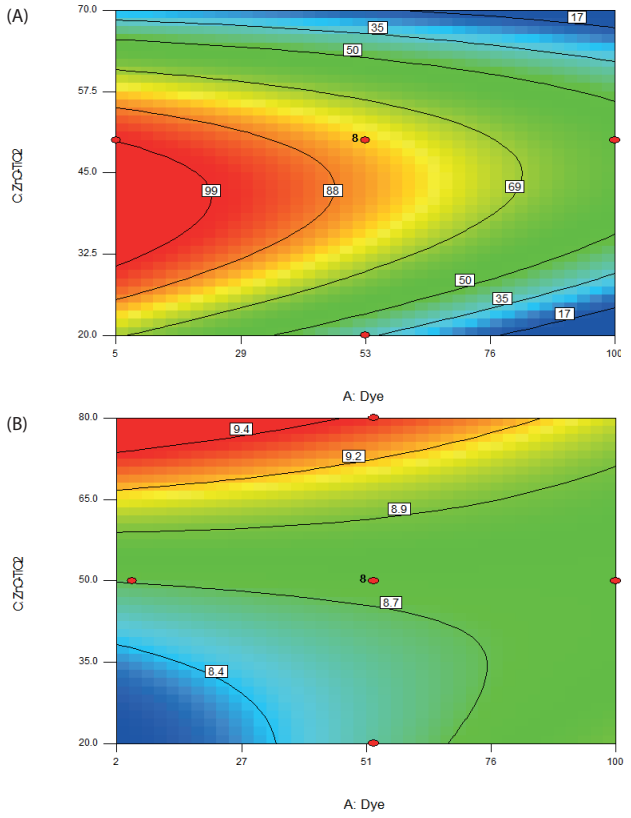


Fig. 5. Effect of initial dye concentration and amount of photocatalysis: (A) DR and (B) pH-out ($t$ = 5 h, Zn:Ti = 0.5%, pH = 7).

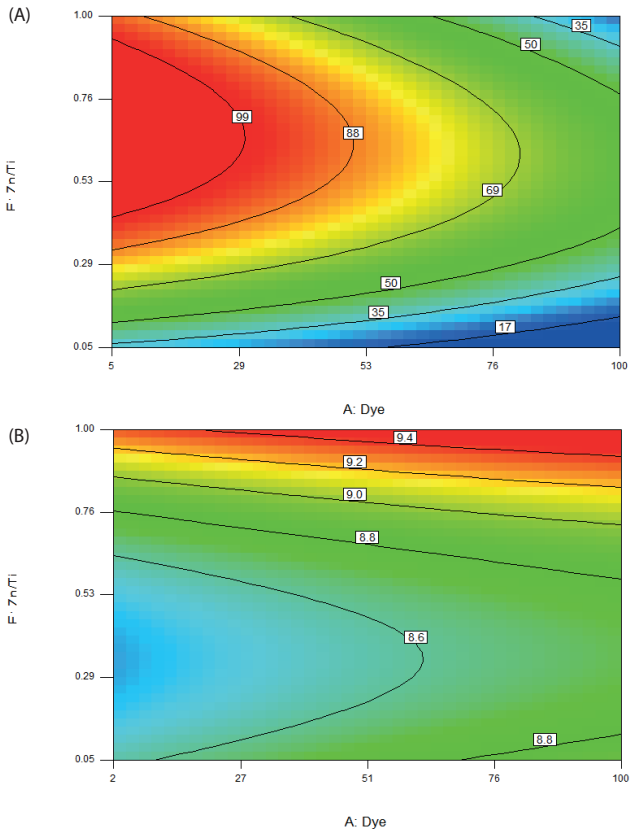


Fig. 6. Effect of initial dye concentration and Zn:Ti: (A) DR and (B) pH-out ($t$ = 5 h, [Zn-$TiO_2$] = 40 g/m$^2$, pH = 7).

Therefore, the surface adsorption of a given dye structure may be more or less in acidic or basic environments, but in general, in the ISO-electric point (point with zero charge), it is minimized [33].

As shown in Fig. 13, anionic dyes investigated in acidic conditions clot [25], and coagulated grains of dye sit on the catalyst surface and cause the photocatalyst operation to malfunction. Even when the efficiency is high, the unremoved dye is deposited on the substrate.

### 3.3.2. Effect of dye concentration

Fig. 14 indicates the effect of the concentration in inconstant conditions with increasing inlet pollutant concentrations ranging from 10 to 100 mg/L in a fixed system. The efficiency decreases from 98% to 50% since the effect of light decreases with increasing dye concentration and the number of active centers on the photocatalyst reduce. Chong et al. [33] and Jiang et al. [28] report similar results in their respective studies.

### 3.3.3. Effect of photocatalyst concentration

According to Fig. 15, by increasing the photocatalyst amount from 20 to 42 g/m$^2$, the dye removal increases from 68% to 90% because the number of active centers on the surface and the absorption amount of photons and pollutants molecules on the catalyst surface increase. However, after increasing the photocatalysts over 42 g/m$^2$, efficiency decreases because agglomerate particles decrease the light absorption on the surface of different locations. Jiang et al.'s [28] study reports the same.

### 3.3.4. Effect of photocatalyst type

The effect of photocatalyst type in constant conditions lasting 6 h, including natural pH dye (6.9), dye concentration of 50 mg/L, and photocatalyst concentration of 44.6 g/m$^2$ with a Zn:Ti ratio equal to 0.53, was investigated and it has been shown in Fig. 16. Removal of dye by glue, $TiO_2$ only, and doped $TiO_2$ reaches 6%, 25%, and 88%, respectively, which indicates the need for a catalyst and confirms the increase in $TiO_2$ photocatalytic activity by dopant.

## 3.4. Optimize the removal conditions

After analyzing the factors affecting the responses, optimization was performed by a central composite design optimization method. The range is determined when color removal above is 90%; dye efficiency degradation is above 67%; and output pH is 9. Fig. 17 shows this range for the natural pH of dye (6.9) at a 6-h duration and 44.6 g/m$^2$ photocatalyst.

After finding the optimal conditions to confirm the model, the test was repeated three times under optimum conditions, and average of results are reported in Fig. 18. This condition contained a pH of 6.9, photocatalyst concentration of 44/6 g/m$^2$, dye concentration of 53 ppm, and Zn/Ti equal

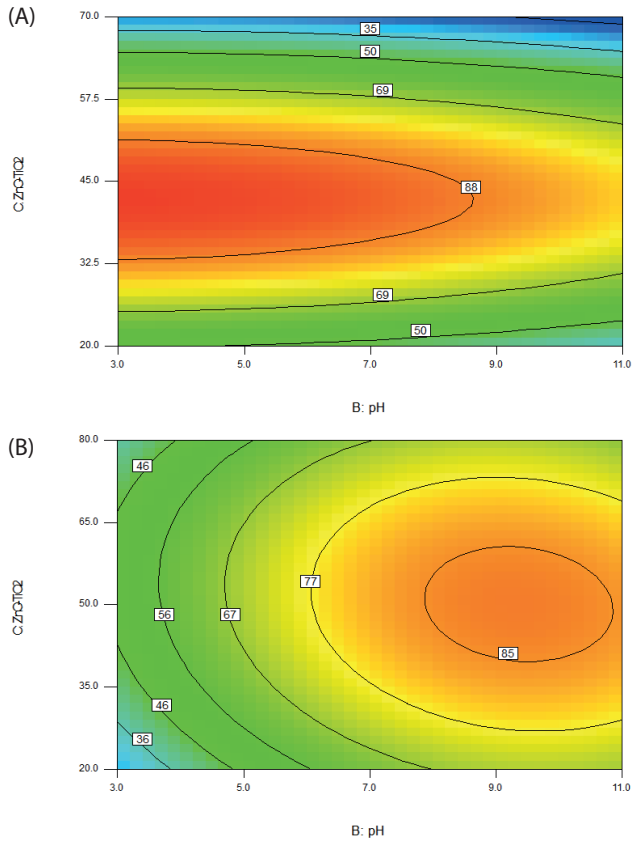


Fig. 7. Effect of amount of photocatalysis and pH: (A) DR and (B) CODR ($t$ = 5 h, Zn:Ti = 0.5%, [Dye] = 40 mg/L).

to 53%. According to the diagram, dye removal efficiency was 87% at 6 h and 90% at 8 h, with a 65% organic load removal.

COD removal efficiency increased at first and then decreased and increased again because the dye had three benzene rings. While the matter was not still perfectly under photocatalytic reaction, it was still hard gradable with low chemical oxygen consumption. After the rings broke, the oxygen consumption required for the reaction to decompose increased. By the end, the simple materials that require less oxygen were formed.

During Fig. 18(C), an output pH of 8.5 was observed at 6 h. With increased time, the effect of doped metal on dye removal increases because there is ample opportunity for response. Additionally, more hydroxyl and oxygen radical are produced because the dye investigated has been anion and buffered, and the output pH increases.

The results, including color removal of 88%, organic load removal of 65%, and output pH of 8.5, compare with the predicted responses at the optimal point, as seen in Table 3. The table also shows that the range of average results occur 95% of the time. Therefore, it can be said that the model of color removal and output pH are acceptable with a 95% confidence level.

### 3.5. Result of liquid chromatography–mass spectrometry

To determine the products under optimal conditions, a liquid chromatography-mass spectrometry (LC-mass) test lasting

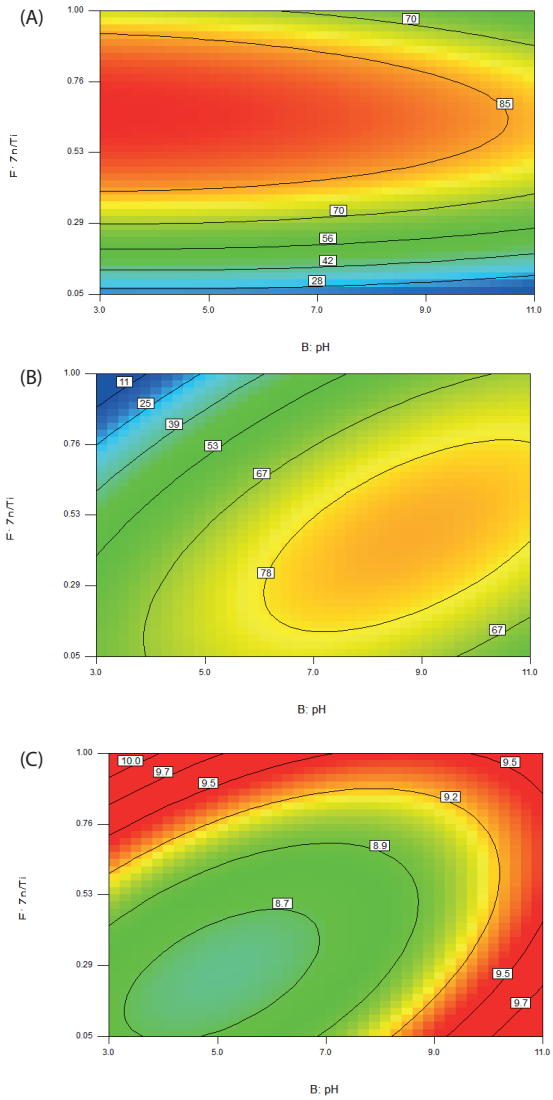


Fig. 8. Effect of pH and Zn:Ti: (A) DR, (B) CODR, and (C) pH-out ($t$ = 5 h, [Zn-$TiO_2$] = 40 g/$m^2$, [Dye] = 40 mg/L).

8 h was carried out in optimal conditions to confirm the model. Standardization of the prototype is presented in Figs. 19(A) and (B). In Fig. 19(B), the rate of mass obtained at the peak point of 59 min is equal to 941.1. This number is related to Direct Blue dye in that four sodium ions are lost and four protons ($H^+$) are taken. The results of the LC-mass test are shown in Figs. 20(A) and (B). As seen in Fig. 20(A), there is no peak at 5.9 min. Next, the mass at this point was determined, and the result is reported in Fig. 20(B). Peak values in these samples indicate poor residual compounds in a solution. It is safe to say that there are no circular complex combinations in the environments and all ingredients are simple in structure. Over time, the complexity of the reaction products reduces, representing the process' ability to reduce effluent toxicity. Intermediate product types during the reaction depend on process steering conditions, such as the initial concentration and reaction time.

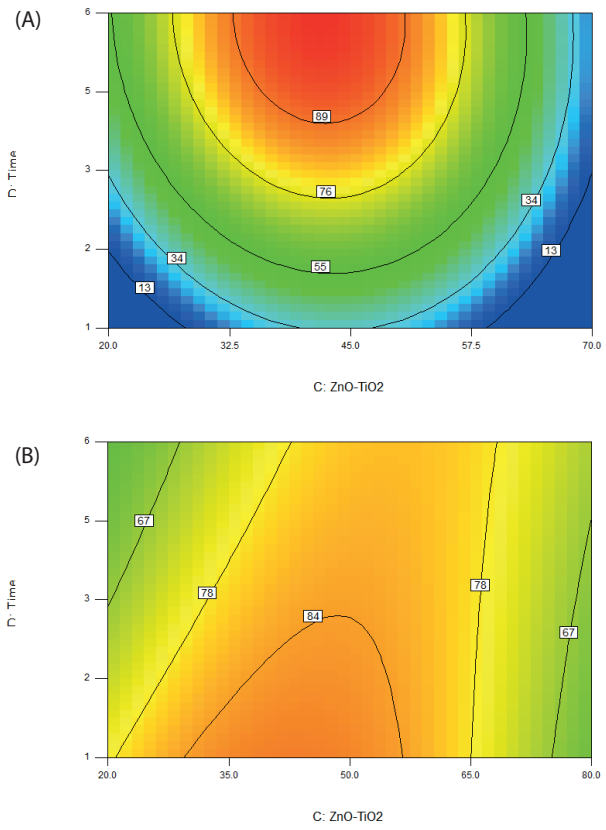


Fig. 9. Effect of time and amount of photocatalysis: (A) DR and (B) COD removed (0.5% Zn-$TiO_2$, pH = 7, [Dye] = 40 mg/L).

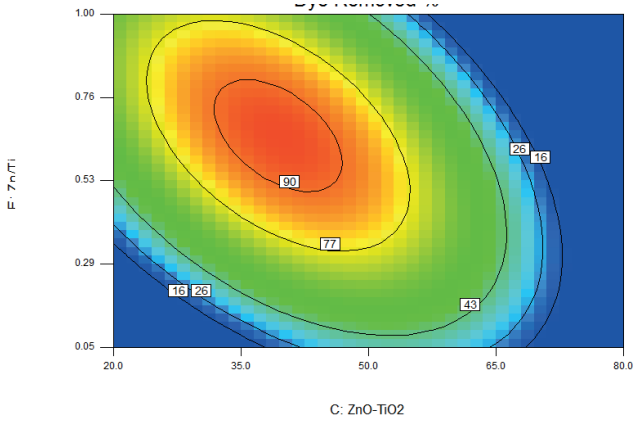


Fig. 10. Effect of Zn:Ti and amount of photocatalysis ($t$ = 5 h, pH = 7, [Dye] = 40 mg/L).

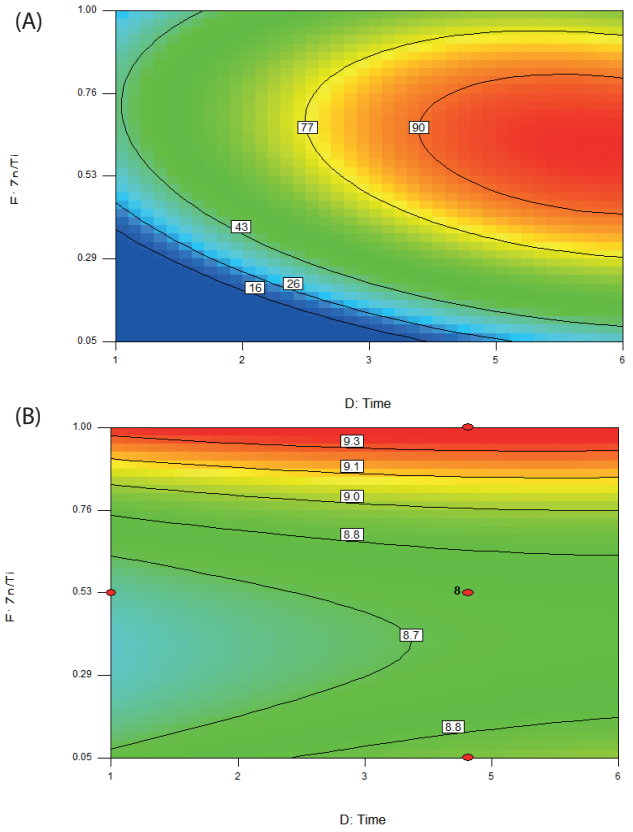


Fig. 11. Effect of Zn:Ti and time: (A) DR and (B) pH-out ([Zn-$TiO_2$] = 40 g/$m^2$, pH = 7, [Dye] = 40 mg/L).

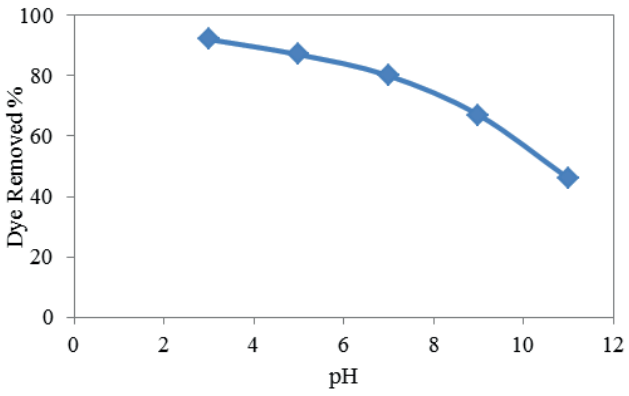


Fig. 12. Effect of pH on dye removal ($t$ = 5 h, [0.5% Zn-$TiO_2$] = 40 g/$m^2$, [Dye] = 50 mg/L).

## 4. Conclusion

The XRD test result shows that the phase transition of the anatase to rutile in doped samples is inhibited; meaning the photocatalytic activity of the doped samples is not more than that of the other samples. The removal of reactions in a continuous solar photo-reactor and in Zn-$TiO_2$ as a photocatalyst was accomplished to analyze the factors affecting efficiency. The test's design was a central composite design, and to ensure the results, the design and experimental testing were performed once. The effects of parameters such as photocatalyst amount, initial pH, pollutant concentration, and zinc to titanium ratio in the dopant construction phase were studied. It was observed that in optimal conditions, including a photocatalyst of 4.6 g/$m^2$, a natural dye pH of 6.9, a dye concentration of 50 mg/L, a duration of 6 h in the sun, and a Zn:Ti ratio equal to 0.53%, dye removal can reach about 90%. Finally, a LC-mass was completed to determine the toxicity of the products produced. The results of these tests indicate destruction of all benzene rings and production of harmless secondary products.

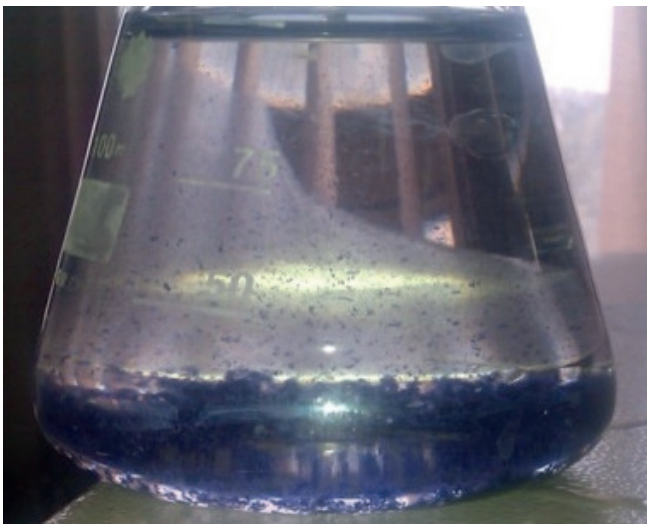

Fig. 13. Clotting dye in acidic conditions.

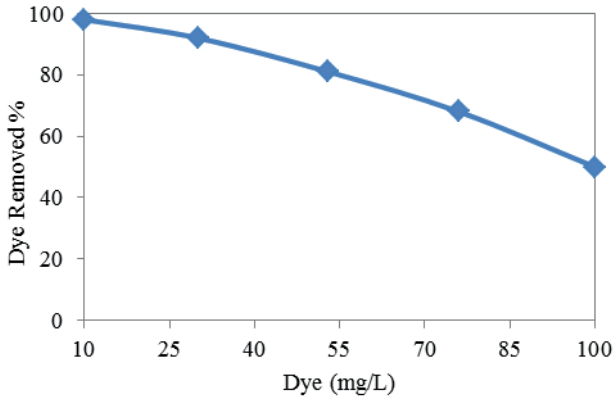


Fig. 14. Effect of dye concentration on dye removal ($t$ = 5 h, [0.5% Zn-$TiO_2$] = 40 g/m$^2$, pH = 7).

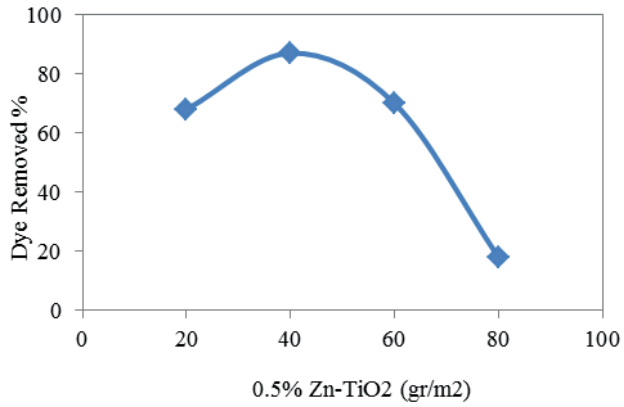


Fig. 15. Effect of photocatalyst concentration on dye removal ($t$ = 5 h, [Dye] = 50 g/m$^2$, Zn:Ti = 0.5%, pH = 7).

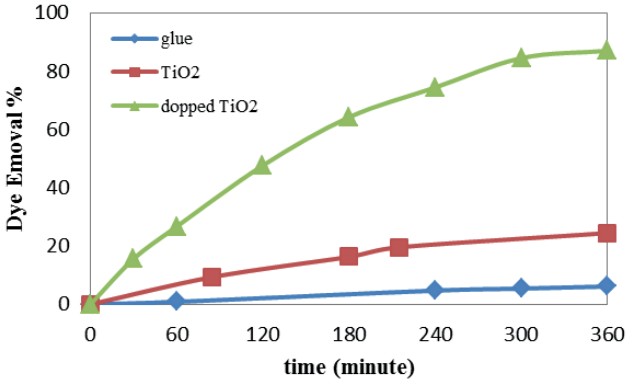


Fig. 16. Effect of photocatalyst type on dye removal ($t$ = 5 h, [Dye] = 50 mg/L, [0.5% Zn-$TiO_2$] = 40 g/m$^2$, pH = 7).

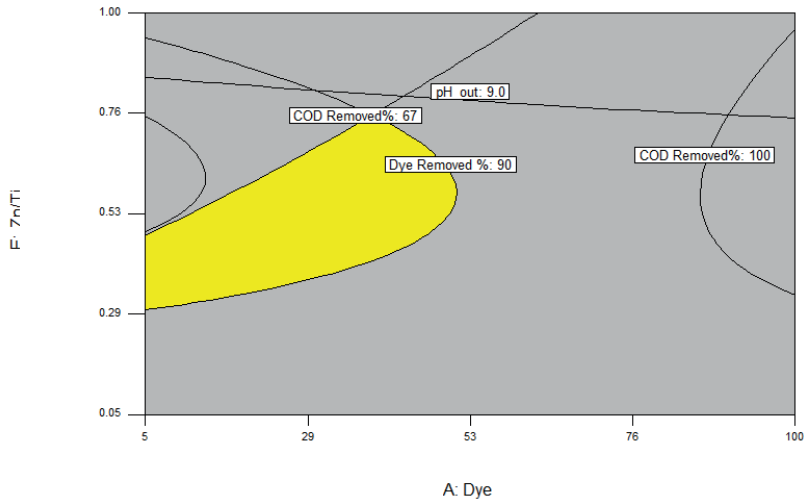


Fig. 17. Range of optimum conditions ($t$ = 5 h, [Zn-$TiO_2$] = 44.6 g/m$^2$, pH = 6.9).

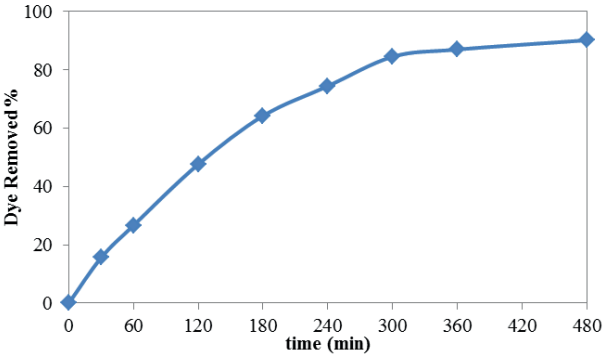


(A)

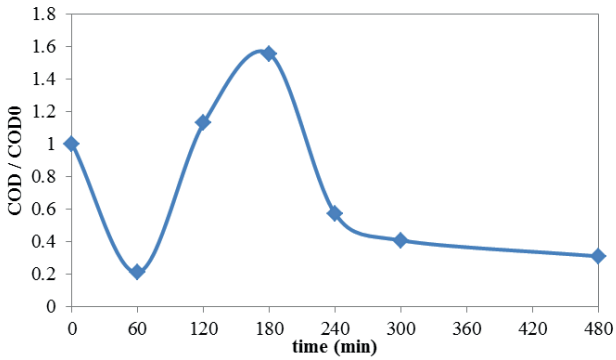


(B)

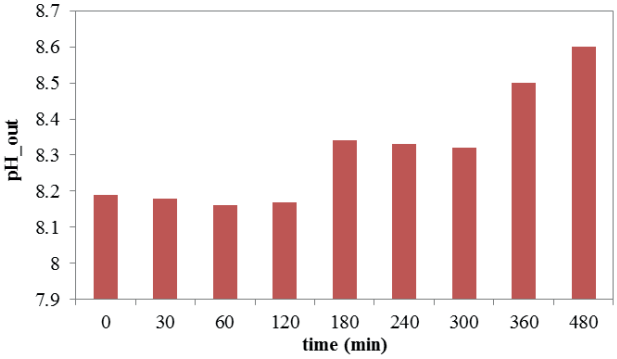


(C)

Fig. 18. The results in optimum condition: (A) DR, (B) CODR, and (C) pH-out (pH = 6.9, [0.53% Zn-$TiO_2$] = 44.6 g/$m^2$, [Dye] = 53 mg/L).

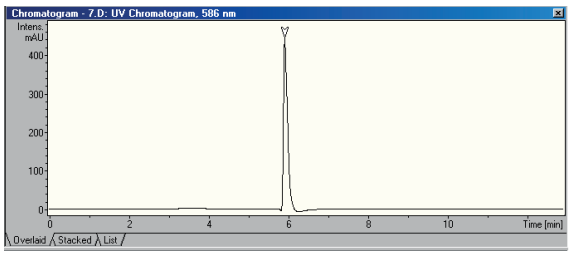


(A)

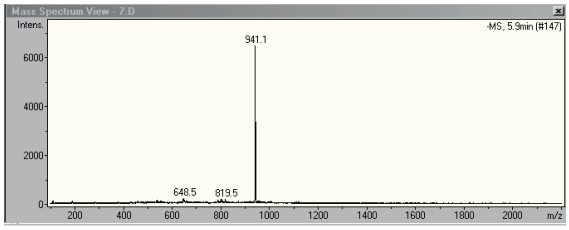


(B)

Fig. 19. Standardization of the pre-sample.

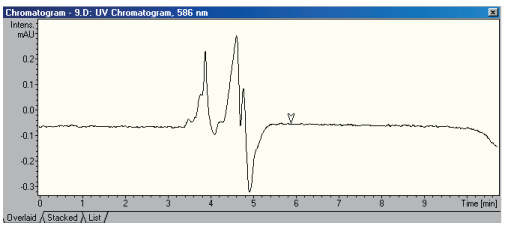


(A)

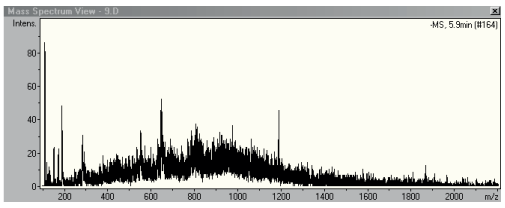


(B)

Fig. 20. Mass of eighth-hour sample.

Table 3
View optimal point

| Result | Prediction | 95% Confidence interval (CI) low | 95% Confidence interval (CI) high | 95% Prediction interval (PI) low | 95% Prediction interval (PI) high |
|---|---|---|---|---|---|
| Dye removed % | 90 | 83.6 | 96.6 | 70 | 110 |
| COD removed % | 84 | 76.2 | 92.2 | 56.4 | 112 |
| pH-out | 8.7 | 8.5 | 8.9 | 8.1 | 9.2 |

**Acknowledgment**

This work was supported in part by the Tarbait Modares University.

**References**

[1] K. Turhan, Z. Turgut, Decolorization of direct dye in textile wastewater by ozonization in a semi-batch bubble column reactor, Desalination, 242 (2009) 256–263.
[2] M.T. Chao, A.R. Mohamed, Roles of titanium dioxide and ion-doped titanium dioxide on photocatalytic degradation of organic pollutants (phenolic compounds and dyes) in aqueous solutions: a review, J. Alloys Compd., 509 (2011)1648–1660.
[3] E. Rossetto, D.I. Petkowicz, H.Z. dos Santos Joao, S.B.C. Pergher, F.G. Penha, Bentonites impregnated with $TiO_2$ for photodegradation of methylene blue, Appl. Clay Sci., 48 (2010) 602–606.
[4] R. Vyas, S. Sharma, P. Gupta, Y.K. Vijay, A.K. Prasad, A.K. Tyagi, K. Sachdev, S.K. Sharma, Enhanced $NO_2$ sensing using ZnO–$TiO_2$ nanocomposite thin films, J. Alloys Compd., 554 (2013) 59–63.
[5] S. Siuleiman, N. Kaneva, A. Bojinova, K. Papazova, A. Apostolov, D. Dimitrov, Photodegradation of Orange II by ZnO and $TiO_2$ powders and nanowire ZnO and ZnO/$TiO_2$ thin films, Colloids Surf., A, 460 (2014) 408–413.
[6] D. Tekin, Photocatalytic degradation of textile dyestuffs using $TiO_2$ nanotubes prepared by sonoelectrochemical method, Appl. Surf. Sci., 318 (2014) 132–136.
[7] M. Černá, M. Veselý, P. Dzik, C. Guillard, E. Puzenat, M. Lepičová, Fabrication, characterization and photocatalytic activity of $TiO_2$ layers prepared by inkjet printing of stabilized nanocrystalline suspensions, Appl. Catal., B, 138–139 (2013) 84–94.
[8] N. Wu, Y. Wang, Y. Lei, B. Wang, C. Han, Flexible N–doped $TiO_2$/C ultrafine fiber mat and its photocatalytic activity under simulated sunlight, Appl. Surf. Sci., 319 (2014) 136–142.
[9] R. Nazari, M. Ebramini, Nano Particles of Titanium Dioxide and Its Applications in Environmental Cleanup, 4th National Biotechnology Congress of Islamic Republic of Iran, Kerman, August, 2005.
[10] M.A. Rauf, M.A. Meetani, S. Hisaindee, An overview on the photocatalytic degradation of azo dyes in the presence of $TiO_2$ doped with selective transition metals, Desalination, 276 (2011) 13–27.
[11] S. Rehman, R. Ullah, A.M. Butt, N.D. Gohar, Strategies of making $TiO_2$ and ZnO visible light active, J. Hazard. Mater., 170 (2009) 560–569.
[12] H.U. Farouk, A.A. Abdul Raman, W.M.A.W. Daud, $TiO_2$ catalyst deactivation in textile wastewater treatment: current challenges and future advances, J. Ind. Eng. Chem., 33 (2016) 11–21.
[13] L.G. Devi, N. Kottam, B.N. Murthy, S.G. Kumar, Enhanced photocatalytic activity of transition metal $Mn^{2+}$, $Ni^{2+}$ and $Zn^{2+}$ doped polycrystalline titania for the degradation of Aniline Blue under UV/solar light, J. Mol. Catal. A: Chem., 328 (2010) 44–52.
[14] L. Narayana, M. Matheswaran, A. Abd Aziz, P. Saravanan, Photocatalytic decolourization of basic green dye by pure and Fe, Co doped $TiO_2$ under daylight illumination, Desalination, 269 (2011) 249–253.
[15] P. Goswami, J.N. Ganguli, Evaluating the potential of a new titania precursor for the synthesis of mesoporous Fe-doped titania with enhanced photocatalytic activity, Mater. Res. Bull., 47 (2012) 2077–2084.
[16] H.-x. Guo, K.-l. Lin, Z.-s. Zheng, F.-b. Xiao, S.-x. Li, Sulfanilic acid-modified P25 $TiO_2$ nanoparticles with improved photocatalytic degradation on Congo red under visible light, Dyes Pigm., 92 (2012) 1278–1284.
[17] A. Yousef, R.M. Brooks, M.M. El-Halwany, N.A.M. Barakat, M.H. EL-Newehy, H.Y. Kim, $Cu_0$-decorated, carbon-doped rutile $TiO_2$ nanofibers via one step electrospinning: effective photocatalyst for azo dyes degradation under solar light, Chem. Eng. Process., 95 (2015) 202–207.
[18] M.R. Delsouz Khaki, B. Sajjadi, A.A. Abdul Raman, W.M.A.W. Daud, S. Shmshirband, Sensitivity analysis of the photoactivity of Cu–$TiO_2$/ZnO during advanced oxidation reaction by Adaptive Neuro-Fuzzy Selection Technique, Measurement., 77 (2016) 155–174.
[19] C. Karunakaran, G. Abiramasundari, P. Gomathisankar, G. Manikandan, V. Anandi, Preparation and characterization of ZnO–$TiO_2$ nanocomposite for photocatalytic disinfection of bacteria and detoxification of cyanide under visible, Mater. Res. Bull., 46 (2011) 1586–1592.
[20] M. Delnavaz, Wastewater Treatment Containing Phenol Using Photo-catalytic Properties with $TiO_2$ Nano-particles Coating on the Concrete Surface, PhD Thesis of Civil and Environmental Engineering, Tarbiat Modares University, Tehran, Iran, 2011.
[21] C. Chen, Z. Wang, S. Ruan, B. Zou, M. Zhao, F. Wu, Photocatalytic degradation of C.I. Acid Orange 52 in the presence of Zn-doped $TiO_2$ prepared by a stearic acid gel method, Dyes Pigm., 77 (2008) 204–209.
[22] M. Khosro Panah, H. Sarpoulaki, S. Kaviani, Examine effect of the thickness of the multilayer coating on photo-catalytic behavior of nano-structured titania coatings on stainless steel 304L, Iranian J. Ceram. Sci. Eng., 3 (2012) 39–55.
[23] L.A. Sarabia, M.C. Ortiz, Response surface methodology, molecular sciences and chemical engineering, Comprehensive Chemometrics, 1 (2009) 345–390.
[24] B.K. Körbahti, M.A. Rauf, Response surface methodology (RSM) analysis of photoinduced decoloration of toludine blue, Chem. Eng. J., 136 (2008) 25–30.
[25] K. Soutsas, V. Karayannis, I. Poulios, A. Riga, K. Ntampegliotis, X. Spiliotis, G. Papapolymerou, Decolorization and degradation of reactive azo dyes via heterogeneous photocatalytic processes, Desalination, 250 (2010) 345–350.
[26] Z.M. El-Bahy, A.A. Ismail, M. Mohamed Reda, Enhancement of titania by doping rare earth for photodegradation of organic dye (Direct Blue), J. Hazard. Mater., 166 (2009) 138–143.
[27] N. Sobana, K. Selvam, M. Swaminathan, Optimization of photocatalytic degradation conditions of Direct Red 23 using nano-Ag doped $TiO_2$, Sep. Purif. Technol., 62 (2008) 648–653.
[28] J. Jiang, Y. Sun, H. Liu, F. Zhu, H. Yin, Solar photocatalytic decolorization of C.I. Basic Blue 41 in an aqueous suspension of $TiO_2$–ZnO, Dyes Pigm., 7 (2008) 77–83.
[29] A.K. Leghari Sajjad, S. Shamaila, B. Tian, F. Chen, J. Zhang, Comparative studies of operational parameters of degradation of azo dyes in visible light by highly efficient WOx/$TiO_2$ photocatalyst, J. Hazard. Mater., 177 (2010) 781–791.
[30] J. Sun, L. Qiao, S. Sun, G. Wang, Photocatalytic degradation of Orange G on nitrogen-doped $TiO_2$ catalysts under visible light and sunlight irradiation, J. Hazard. Mater., 155 (2008) 312–319.
[31] J. Wang, Y. Lv, Z. Zhang, Y. Deng, L. Zhang, B. Liu, R. Xu, X. Zhang, Sonocatalytic degradation of azo fuchsine in the presence of the Co-doped and Cr-doped mixed crystal $TiO_2$ powders and comparison of their sonocatalytic activities, J. Hazard. Mater., 170 (2009) 398–404.
[32] T.B. Nguyen, M.-J. Hwang, K.-S. Ryu, Synthesis and high photocatalytic activity of Zn-doped $TiO_2$ nanoparticles by sol-gel and ammonia-evaporation method, Bull. Korean Chem. Soc., 33 (2012) 243–247.
[33] M.N. Chong, B. Jin, C.W.K. Chow, C. Saint, Recent developments in photocatalytic water treatment technology: a review, Water Res., 44 (2010) 2997–3027.